PHYSICAL REVIEW A VOLUME 19, NUMBER 1 JANUARY 1979

Impact-parameter-dependent inner-shell vacancy production in 0.7–2.7 MeV/amu $^{58}_{28}$Ni collisions with $_{25}$Mn, $_{50}$Sn, and $_{82}$Pb

B. M. Johnson, K. W. Jones, and Werner Brandt*
Brookhaven National Laboratory, Upton, New York 11973

F. C. Jundt and G. Guillaume
Centre de Recherches Nucléaires et Université Louis Pasteur, Strasbourg, France

T. H. Kruse
Rutgers University, New Brunswick, New Jersey 08903
(Received 5 January 1978; revised manuscript received 7 August 1978)

Impact-parameter-dependent probabilities of K and L characteristic x-ray production in collisions of 45-, 94-, and 138-MeV $^{58}_{28}$Ni ions with solid targets of $_{25}$Mn, $_{50}$Sn, and $_{82}$Pb were measured. The results are compared with predictions of the statistical and the molecular-orbital models for inner-shell vacancy production. A short development of the statistical model in a random-walk approximation is given to display the physical content of the model in simple terms.

I. INTRODUCTION

Measurements of the cross sections for production of characteristic x rays in heavy ion-atom collisions have been in progress for many years. Detailed knowledge of the systematics of these collisions as a function of projectile atomic number Z_1, target atomic number Z_2, and the laboratory kinetic energy of the projectile E, derives from the production of K-shell x rays. Total K-vacancy cross-section measurements have been made in several experiments with solid targets. Kubo *et al.*[1] reported target and projectile cross sections for $_{28}$Ni and $_{35}$Br beams as a function of Z_2 at several projectile energies and observed strong variations in the cross section which are attributed to electronic-shell effects. Meyerhof *et al.*[2] carried out similar experiments with beams of $_{35}$Br, $_{36}$Kr, $_{53}$I, $_{54}$Xe, and $_{82}$Pb at energies up to 470 MeV. Cross sections at low energies were reported by Jones *et al.*[3] for 5-MeV $_{10}$Ne and $_{18}$Ar beams. A common trend for given Z_1 is the strong variation of total K-shell-vacancy production as a function of Z_2. Measurements of the probability P_K of vacancy production as a function of impact parameter b have been reported for relatively light ions and targets.[4-6] Recently, experiments by Johnson *et al.*[7] with a $_{28}$Ni beam on solid $_{25}$Mn and $_{82}$Pb targets and Cocke *et al.*[8] with a $_{17}$Cl beam on a gaseous $_{18}$Ar target have started to give information for ranges of higher Z_1, Z_2, and E, where total cross-section measurements have been performed.

The mechanisms for vacancy production in atomic collisions are complex and can range between two limiting cases. On the one hand is the production of a K vacancy by direct Coulomb ionization caused by the Coulomb field of a completely stripped projectile.[9] On the other is the vacancy production during the interaction of the electron clouds of the projectile and target atoms, Pauli excitation,[10] or as a result of the formation of a quasimolecule, the Fano-Lichten model.[11,12] Under such conditions, the cross sections are usually much larger than direct Coulomb-excitation cross sections.

The Fano-Lichten molecular-orbital (MO) model has been developed by Briggs and Macek[13] and by Taulbjerg *et al.*[14] to give detailed predictions of the impact-parameter dependence of ionization probabilities, and of the scaling of the total cross sections. This approach requires specific assumptions about a few orbitals taken to be prevalent in a given collision. In collisions involving a large number of molecular-orbital crossings, the vacancy production can be studied in terms of a statistical model, first developed from a diffusion-equation approach by Mittleman and Wilets[15] for total ionization. This approach has been applied by Brandt and Jones[5] to K-vacancy production. A simple development based on random walk between level crossings can also be used to illuminate the physical content of the model. The statistical model is effective in representing differential and total cross-section data on disparate collision systems in a concise manner.[7,16]

The present experiment was undertaken to extend the work of Johnson *et al.*[7] by measuring the impact-parameter-dependent probability of inner-shell-vacancy production by 45–138-MeV $_{28}$Ni beams on $_{25}$Mn, $_{50}$Sn, and $_{82}$Pb solid targets. The targets were chosen because the corresponding total cross sections represent maxima (Mn, Pb) and a minimum (Sn) in the Z_2 dependence of the

Ni measurements of Kubo *et al.*[1] The experimental results are discussed in terms of the statistical model and are compared with predictions of the molecular-orbital model.

II. EXPERIMENTAL PROCEDURE

Beams of $^{58}_{28}$Ni ions at 45, 94, and 138 MeV were obtained from the Brookhaven MP–tandem Van de Graaff accelerator facility with currents in the range of 1–10 nA/ion charge. The beam was collimated with two 0.25-mm-diam apertures spaced 20 cm apart, followed by a 0.5-mm-diam scraper slit at a distance of 6 cm, limiting the beam dispersion to at most 0.15°. Targets were prepared by vacuum evaporation of natural $_{25}$Mn and $_{82}$Pb in films of 20 μg/cm^2, and $_{50}$Sn in films of 100 μg/cm^2 with uncertainties in target thickness of ±20%, onto 20-μg/cm^2 carbon foils. They were positioned 8 cm downstream from the scraper slit and inclined at an angle of 45° to the beam direction.

After passing through the target material and the supporting carbon foil, the beam was stopped in a small Faraday cup mounted at the center of an annular particle detector. The cup current to ground was used for monitoring the accelerator operation. The annular particle detector consisted of a 0.5-mm-thick collimator with inner radius 4.0 mm and outer radius 4.8 mm positioned in front of a silicon surface-barrier detector with a sensitive depth of 100 μm and an active area of 200 mm^2. The mean scattering angle subtended by the collimator was varied by moving the detector assembly coaxially with the beam direction on a sliding shaft. At the minimum and maximum target-to-detector distances of 3.3 and 53 cm, particles were detected that had been scattered through angles $(7.5 \pm 1)°$ and $0.5 \pm 0.1)°$, respectively. The range of accepted scattering angles resulted in detection of scattered particles which had undergone collisions with the target atoms over a range of impact parameters approximately ±10% of the calculated mean value. The solid angle of the detector was reduced at small distances by the finite thickness of the collimator rings for which corrections were made. The energy resolution of the surface-barrier detector deteriorated with radiation damage, but the results of the experiment were insensitive to this resolution, as demonstrated in repeated runs with used and new particle detectors under otherwise equal conditions.

A liquid-nitrogen-cooled Si(Li) x-ray detector with an active area of 80 mm^2 and an energy resolution of 200 eV for the 5.9-keV $K\alpha$ line of Mn registered x rays produced during the passage of the beam through the target. The 25.4-μm beryllium window of the detector was directly coupled to the vacuum chamber at a distance of 2.5 cm from the target at 90° to the incident beam. A calibrated $^{55}_{26}$Fe x-ray source at the target position determined the value of the product of acceptance solid angle and detection efficiency for the x-ray detector at the 5.9-keV Mn $K\alpha$ x-ray energy. Corrections were made for changes in the transmission of the Be entrance window for Ni, Sn, and Pb x rays, and for Al absorbers placed between the detector and the Sn, and Pb targets to reduce the counting rate from radiative electron capture and low-energy L and M x rays.

Signals from the preamplifiers of the x-ray and particle detectors were split to handle separately the circuitry for the x-ray and particle coincidences, and for the high-resolution energy spectra. The start and stop pulses for a time-to-pulse-height converter were derived from timing filter amplifiers followed by constant-fraction timing discriminators. Their levels were set to accept particles scattered in the target films and x rays emitted from the projectile and target atoms. Coincident x rays from projectile and target atoms were recorded through gates derived from the high-resolution x-ray circuitry. A typical time resolution was 20 nsec for the 7.5-keV Ni $K\alpha$ x ray.

The probability P_K or P_L for producing a K- or L-shell vacancy was calculated for each detector position from the relationship $P = 4\pi N_C / N_S \gamma \Omega_x \epsilon_x$, where N_C is the number of coincidences, N_S the number of scattered particles, γ the static fluorescence yield,[17] and $\Omega_x \epsilon_x$ the solid-angle efficiency for the x-ray detector. The x rays from the beam and target were taken to be emitted isotropically.

Although it was not the primary aim of the experiment, it was also possible to measure total vacancy-production cross sections at each detector position. The agreement of these values with previous measurements[1] established the validity of the calibration for the absolute values of P_K and P_L. The cross sections σ_K or σ_L were calculated from the relationship

$$\sigma = \frac{4\pi N_x}{N_S \gamma} \left(\frac{d\sigma}{d\Omega}\right)_S \frac{\Omega_S \epsilon_S}{\Omega_x \epsilon_x},$$

where N_x is the number of x rays, $(d\sigma/d\Omega)_S$ the appropriate cross section for scattering particles into the particle detector, and $\Omega_S \epsilon_S$ the solid-angle efficiency for the particle detector. The mean values of σ obtained from this procedure are listed in Table I.

Data taken with bare carbon foils showed that Ni x-ray emission at 45 MeV was negligible. At

TABLE I. Total inner-shell-vacancy-production cross sections σ_K or σ_L in cm^2. Data listed under experiment I are from this work, and data under II are from Ref. 1 with mean experimental uncertainties of ±30%. Theoretical values are calculated from Eq. (4) with the listed constants D_K, D_L, and R_0 as obtained by fitting Eq. (1) to the experimental probabilities P_K and P_L shown in Figs. 1–6. Theoretical values for $\sigma_K(L)$ and $\sigma_K(H)$ for $_{28}$Ni+$_{25}$Mn collisions were obtained by calculating σ_K according to Eq. (4) and applying the charge-sharing formalism of Ref. 21 to $\sigma_K = \sigma_K(L) + \sigma_L(H)$. Numbers in parentheses are powers of 10.

Collision pair	Observed x rays	Cross-section Identification	D_K or D_L (cm^2/sec)	R_0 (cm)	$\sigma_K/2$ or $\sigma_L/8$ (cm^2) E_1 = 45 MeV Experiment I	E_1 = 45 MeV Experiment II	E_1 = 45 MeV Theory	94 MeV Experiment I	94 MeV Experiment II	94 MeV Theory	138 MeV Experiment I	138 MeV Theory
$_{28}$Ni+$_{25}$Mn	Ni K	$\sigma_K(H)$		1.1(−9)	2.0(−21)	5.7(−21)	4.8(−21)	1.7(−20)	2.0(−20)	1.8(−20)	3.9(−20)	3.2(−20)
$_{28}$Ni+$_{25}$Mn	Mn K	$\sigma_K(L)$		1.1(−9)	1.0(−20)	1.3(−20)	2.4(−20)	4.2(−20)	2.2(−20)	5.5(−20)	5.0(−20)	7.9(−20)
$_{28}$Ni+$_{25}$Mn	Ni K + Mn K	$\sigma_K(T)$	19	1.1(−9)	1.2(−20)	1.9(−20)	2.9(−20)	5.9(−20)	4.2(−20)	7.3(−20)	8.9(−20)	1.1(−19)
$_{28}$Ni+$_{50}$Sn	Ni K	$\sigma_K(T)$	35	9.8(−10)	6.0(−22)	3.6(−22)	1.2(−21)	7.0(−21)	4.5(−21)	6.6(−21)	1.0(−20)	1.2(−20)
$_{28}$Ni+$_{82}$Pb	Ni K	$\sigma_K(T)$	21	8.8(−10)	1.2(−20)	5.0(−21)	5.8(−21)	8.0(−20)	2.3(−20)	2.1(−20)	1.5(−19)	5.8(−20)
$_{28}$Ni+$_{50}$Sn	Sn L	$\sigma_L(H)$	14	9.8(−10)	3.4(−21)	1.9(−20)	3.6(−20)	2.3(−20)	5.9(−20)	8.8(−20)	3.6(−20)	1.4(−19)
$_{28}$Ni+$_{82}$Pb	Pb L	$\sigma_L(H)$	39	8.8(−10)	2.1(−21)	3.5(−22)	2.4(−22)	2.5(−21)	1.1(−21)	2.1(−21)	3.0(−21)	4.9(−21)

the higher beam energies, 94 and 138 MeV, appreciable beam x-ray production was observed and the data were corrected for contributions from the carbon backing.

The effects of multiple scattering in the target were estimated from the theory of Meyer.[18] We conclude that multiple scattering should not affect the results compared to instrumental uncertainties at scattering angles greater than a few degrees corresponding to the small impact parameters. At small angles corresponding to the large impact parameters multiple scattering becomes significant. The value of P at the largest impact parameter was taken to be indicative of contributions from multiple scattering and long-range processes such as direct Coulomb ionization.

Inner-shell-vacancy production in heavy ion-atom collisions can be influenced by the degree of ionization and particular electronic configurations of the collision partners. It has been shown[19] that in general many electrons are removed in a single close collision, resulting in a distribution of final charge states and electronic configurations even though the initial states are well defined. The collision system is also inevitably perturbed by the acceleration process which depends on the use of rather heavily ionized projectiles. The study of single collisions with the use of a gas target must then serve to illuminate some aspects of the collision process, but the use of the gas target is not necessarily preferable or required. Solid targets are used here since they offer greater flexibility in the choice of collision pairs and since for the Ni-Mn case prior formation of $2p\pi$ (Ni $2p$) vacancies serves to help decouple that production mechanism from the $2p\pi$-$2p\sigma$ rotational coupling mechanism which forms the basis of quantitative MO calculations.[13,14] Formation of the $2p\pi$ vacancies is predominantly at large impact parameters and will not affect the measured impact-parameter dependence of K vacancies at small impact parameters. Absolute values for the cross sections are not of crucial interest since we are primarily concerned with the shape of the impact-parameter dependence.

The mean charge state of the nickel projectile in the target varies from about 15 to 20 for the bombarding energies used in the experiment. Such a change may enhance the number of $2p\pi$ vacancies for the Ni-Mn system and could result in a related energy-dependent enhancement of the cross section. Again, the impact-parameter dependence will not be affected appreciably by the large impact-parameter ionization events.

For the Sn and Pb targets the molecular orbitals

contributing to K- and L-vacancy formation correspond to atomic orbitals of the target and not the nickel projectile. Here the use of solid targets should have little or no influence on the results aside from the multiple-scattering effects discussed above. The influence of the use of solid targets on experiments of this type has also been discussed by Tserruya *et al.*[16] who reached similar conclusions.

III. DISCUSSION

Heavy ion-atom collisions in general are expected to be characterized by a distribution of charge and electronic states in a quasimolecular system with complex and densely spaced level crossings. Following the first attempt,[6] the data are discussed in terms of the statistical model which is especially appropriate for complex collision systems. The effects of various electronic configurations and the complexity of the collision are incorporated in one adjustable parameter of the model, which scales in the atomic numbers of the collision pair.

A detailed treatment of the time-dependent diffusion problem of excitation to the continuum for total ionization was given by Mittleman and Wilets.[15] It was developed for inner-shell ionizations and applied to K shells by Brandt and Jones.[6] It is used here for the first time to interpret L-shell data. In the diffusion model the probability for vacancy production per electron in the n shell is given by

$$P_n(b) \approx 1 - \frac{2}{\pi} \sum_{\nu=0}^{\infty} \frac{(-1)^\nu}{\nu + \frac{1}{2}} \exp\left[-(\nu + \tfrac{1}{2})\pi^2 s_n(b)\right], \tag{1}$$

where

$$s_n(b) = \frac{2R_0 v}{D_n} F\left(\frac{b}{R_0}\right) = w_n F(x), \tag{2}$$

with

$$F(x) = \left[(1-x^2)^{1/2} - x \arccos x\right]\theta(1-x^2), \tag{3}$$

with the notation $w_n = (2R_0 v_n / D_n)(v/v_n)$, where D_n is the diffusion constant. The total vacancy production cross section becomes

$$\sigma_n = 2\pi \int_0^{R_0} P_n(b) b\, db = \pi R_0^2 S(w_n), \tag{4}$$

where the function $S(w_n)$ is given in Ref. 15. The coefficient D_n contains in principle all the quantum-mechanical information about electron promotion between interacting level crossings in the molecular-orbital picture. In particular, D_n changes with ϵ_n, the gap from the level n in the combined atom to unoccupied states which can be affected by the degree of ionization and by vacnacies in the core of the projectiles as they are prepared, prior to the collision, by the conditions of the experiment and may be affected during the time of strong interaction. The interaction radius has been chosen as the Thomas-Fermi radius of the united atom and has not been used as an adjustable parameter to be extracted from the data. In this form we expect the statistical model to give a fit to the general trend of the data, but it is not expected to fit all small variations.

The development of the statistical model by Mittleman and Wilets,[15] as used, here treats vacancy production as the diffusion in energy space of a vacancy from an unoccupied level through a number of interacting level crossings of transient molecular orbitals to some inner shell of the united atom. This approach requires an extreme assumption about the density of molecular orbitals which is, in fact, not necessary. Alternatively, a vacancy can be viewed as being produced in the inner shell by a random-walk process. It can be shown rather simply from this random-walk assumption that results for the impact-parameter dependence and total cross section are obtained which are essentially identical to Eqs. (1)–(4). A short derivation of this result is given in the Appendix. Since a random-walk process quickly approaches a statistical limit even for a small number of steps, the results of the theory are not sensitive to the detailed form of the density of level crossings. The random-walk approach is perhaps physically a more reasonable framework for discussion of inner-shell-vacancy formation than a diffusion picture. That the level density is not a crucial factor is in agreement with a conjecture by Wilets[20] who found that the value for the diffusion parameter is independent of level density to first order.

The main results of the experiment are shown in Figs. 1–6. The uncertainties due to counting statistics are indicated. Total cross sections are given in Table I. The K-shell data for P and σ are divided by 2, the number of electrons in the shell, and reported in the form of the summed probabilities $P_K(L) + P_K(H)$, and summed cross sections $\sigma_K(L) + \sigma_K(H)$, per K-shell electron. The notation (L) and (H), respectively, refers to the light and heavy members of the collision pairs. Ionization probabilities and cross sections for the individual collision partners in nearly symmetric collisions can be culled by use of the Meyerhof charge-sharing formalism.[21] The variation with impact parameter for the Mn, Sn, and Pb targets seem to be very similar in Figs. 1–3. Apparently the differences in reaction mechanisms which

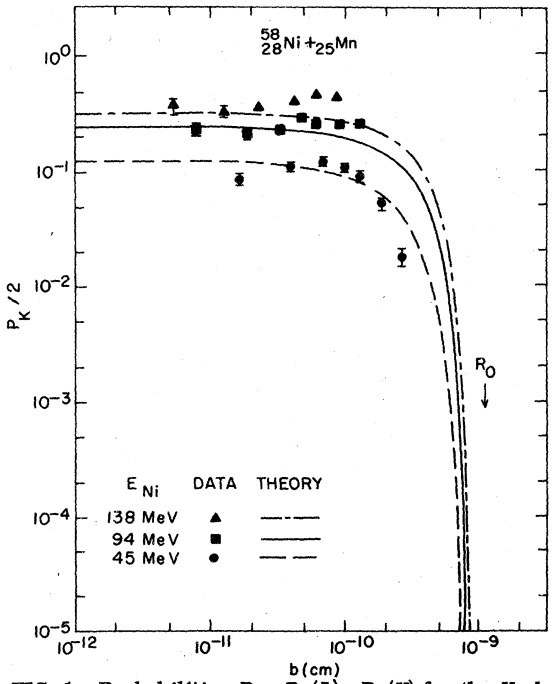

FIG. 1. Probabilities $P_K = P_K(L) + P_K(H)$ for the K-shell vacancy production in light (L) and heavy (H) collision partners, for $_{28}Ni+_{25}Mn$ as a function of impact parameter b for three collisions energies. The curves present the predictions of the statistical model, with the diffusion constant D_K and interaction radius R_0 listed in Table I.

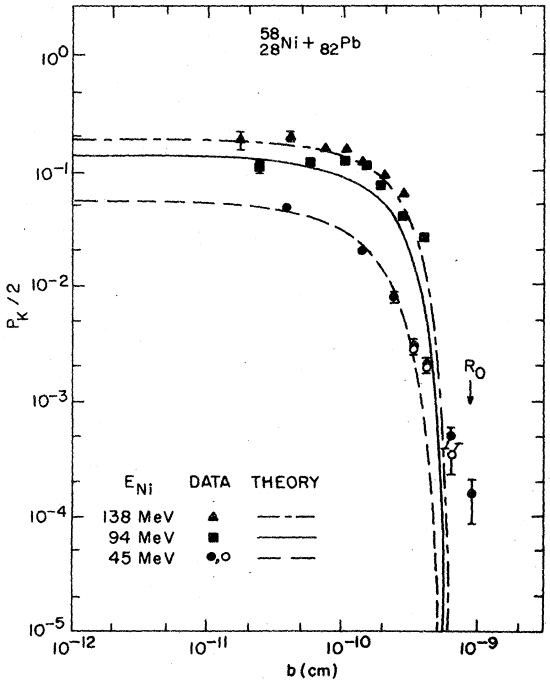

FIG. 3. K-shell-vacancy-production probabilities $P_K \equiv P_K(L) + P_K(H) \simeq P_K(L)$ for $_{28}Ni+_{82}Pb$ as a function of impact parameter b for three collision energies. The curves present the predictions of the statistical model with D_K and R_0 listed in Table I.

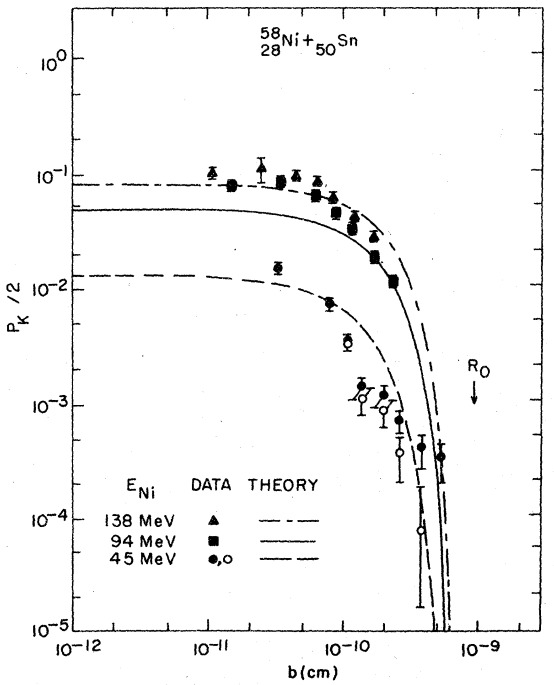

FIG. 2. K-shell vacancy-production probabilities $P_K \equiv P_K(L) + P_K(H) \simeq P_K(L)$ for $_{28}Ni+_{50}Sn$ as a function of impact parameter b for three collision energies. The curves present the predictions of the statistical model with D_K and R_0 listed in Table I.

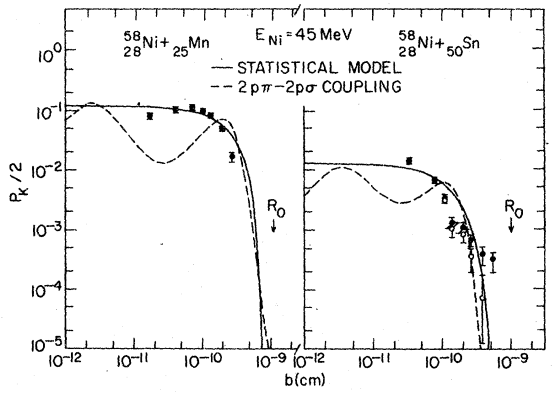

FIG. 4. Comparison of experimental K-shell ionization probabilities P_K for $_{28}Ni+_{25}Mn$ and $_{28}Ni+_{50}Sn$ at 45 MeV with the predictions of the statistical and molecular-orbital models. Data and solid curves are from Figs. 1 and 2. Vertical bars represent uncertainties in counting statistics. Solid curves: predictions of the statistical model with D_K and R_0 as listed in Table I; dashed curves: predictions based on $2p\pi$-$2p\sigma$ MO coupling from Ref. 14 averaged over the range of impact parameters accepted at each position of the annular detector. For normalization, the number $2p\pi$ vacancies was determined from the measured total cross section.

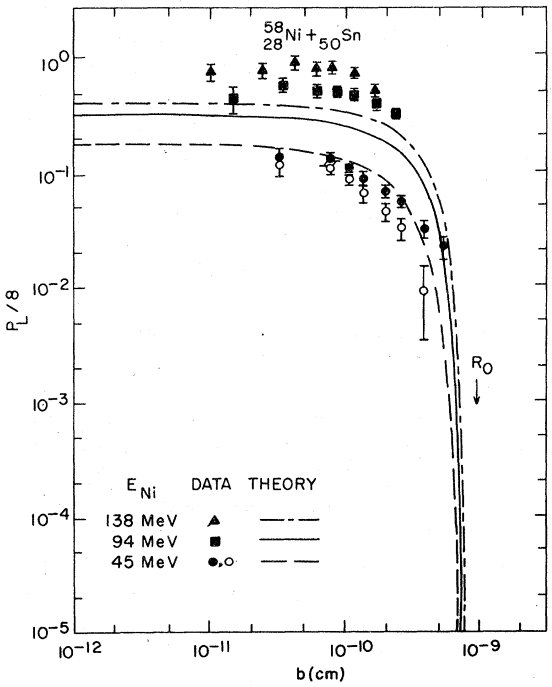

FIG. 5. L-shell-vacancy-production probabilities $P_L = P_L(H)$ for $_{28}Ni + _{50}Sn$ as a function of impact parameter b for three collisions energies. The curves present the predictions of the statistical model with D_L and R_0 listed in Table I.

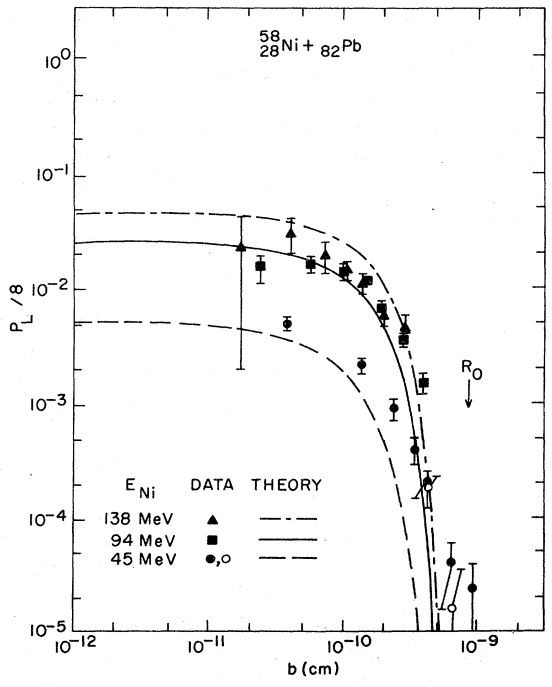

FIG. 6. L-shell-vacancy-production probabilities $P_L = P_L H)$ for $_{28}Ni + _{82}Pb$ as a function of impact parameter b for three collision energies. The curves present the predictions of the statistical model with D_L and R_0 listed in Table I.

cause the Z_2-dependent structure in the total cross-section data of Kubo *et al.*[1] are mainly reflected in the magnitudes of P_K, but not in the variation of P_K with impact parameter. There is some weak evidence for additional structure in the 45-MeV data which deserves further study.

We present in Figs. 5 and 6 the L-shell data in a similar manner by dividing the measured $P_L(H)$ and $\sigma_L(H)$ by 8, the number of electrons in the L shell. The magnitudes found for $\sigma_L(H)$ and the dependence of $P_L(H)$ on impact parameter and bombarding energy are similar to those observed for the K-shell-vacancy production.

Figures 1–6 compare the impact-parameter-dependent data with the statistical-model predictions via Eqs. (1)–(3). In order to be definite, R_0 is set equal to the Thomas-Fermi radius of the combined atom, $R_0 = 0.885\, a_0 Z_{\text{eff}}^{-1/3}$ with $Z_{\text{eff}} = (Z_1^{2/3} + Z_2^{2/3})^{3/2}$ and $a_0 = 0.0529$ nm. The diffusion coefficients D_K and D_L were chosen to achieve a best fit to the experimental data and are listed in Table I together with the experimental and calculated Eq. (4) total cross sections. Inspection of the figures shows that the particular choice of R_0 does not affect sensitively the curves calculated according to Eq. (1) in the range of b, where the ionization probabilities are large. In fact, if the P values at the largest impact parameters in Figs. 2–6 are taken to be indicative of the contributions from multiple-scattering and long-range processes such as direct Coulomb ionization, and are subtracted (open circles), the experimental ionization probabilities for the smaller impact parameters drop towards zero as the b values approach R_0, consistent with the simple form of Eq. (3).

Values for D_K in nearly symmetric collisions are expected to have the form $D_K = [(Z_1 + Z_2)/A]^{\alpha}(\hbar/m)$, where A and α are parameters weakly dependent on Z_1 and Z_2. In the validity range of the statistical model the exponent α is expected to have values near 2.[6] For this α value, the D_K values in Table I indicate that $A \approx 13$ for $_{28}Ni + _{25}Mn$ and $A \approx 14$ for $_{28}Ni + _{50}Sn$. For the most asymmetric collision, $_{28}Ni + _{82}Pb$, D_K is smaller, corresponding to $A \approx 26$. The values of D_K for Mn and Pb targets are in reasonable agreement with our earlier work at a single bombarding energy of 45 MeV.

It should be emphasized that the number and values of D_K just cited are found by comparing our experimental data with the values of $P(b)$ predicted in Eqs. (1)–(3). Early work[5] on limited ranges of light atoms and in nearly symmetric collisions $Z_1 \approx Z_2$ was described by D_K given by

$$D_K \simeq [\tfrac{1}{18}(Z_1 + Z_2)]^3 \hbar/\mathrm{m}\,.$$

It can be equally well represented by

$$D_K = [\tfrac{1}{12}(Z_1 + Z_2)]^2 \hbar/m,$$

consistent with the present work. The value of the diffusion parameter should be adjusted to fit the data and then compared to these systematics which are an average through many different experimental results and are not a prediction of the theory.

We also analyzed the P_K data for 45-MeV $_{28}$Ni ions on $_{25}$Mn and $_{50}$Sn targets in terms of the MO model.[13,14] Vacancies in the $2p\pi$ orbital brought into the collision are transferred to the $2p\sigma$ orbital by rotational coupling and so produce K-shell vacancies in the light member of the interacting pair. Vacancies in the K shell of the heavy atom can be produced by radial coupling between the $2p\sigma$ and $2p\pi$ orbitals. The dashed curves in Fig. 4 were calculated using the universal table and scaling laws of Taulbjerg *et al.*[14] and normalized to fit the measured total cross section. The disagreement with the P_K data is consistent with the observations of Tserruya *et al.*[16] for $_{17}$Cl-$_{17}$Cl and $_{17}$Cl-$_{22}$Ti solid-target collisions, but in contrast to the gas-target collision of $_{17}$Cl-$_{18}$Ar, where Cocke *et al.*[8] found agreement with these predictions. For comparison the statistical-model curves from Figs. 1 and 2 are included as solid curves.

The theoretical fits to the P_L data shown in Figs. 5 and 6 were obtained by adjusting the value of D_L without changing the choice of the Thomas-Fermi radius for the interaction range R_0. The general shape of P_L as a function of impact parameter is well reproduced. The predicted energy dependence of P_L is somewhat weaker than that displayed by the experiments. This could represent a stronger dependence of P_L on the charge state of the incident ion than was observed for P_K. The use of the statistical model permits a unified description of the production of different types of vacancies in ion-atom interactions and illustrates the unique power of the theory in collating different types of experimental data.

IV. SUMMARY AND CONCLUSIONS

We have reported inner-shell-vacancy production probabilities P_K and P_L, and total cross sections σ_K and σ_L, derived from x-ray production measurements for $Z_1 = 28$ ions on solid targets with $Z_2 = 25$, 50, and 82. The impact-parameter dependence of the P_K and P_L data can be represented well by the statistical model through the choice of two parameters in the diffusion coefficient for all collision pairs. Given these diffusion coefficients, the statistical model predicts accurately the values of the measured K- and L-shell cross sections. Over the range of impact parameters studied, the $2p\pi$-$2p\sigma$ MO rotational-coupling model does not reproduce the shape of the P_K data for Ni-Mn and Ni-Sn collisions where this model should be applicable. Although Cocke *et al.*[8] found agreement with this model for Cl-Ar collisions, similar disagreement was observed by Tserruya *et al.*[16] for Cl-Cl and Cl-Ti collisions.

Our results, then, extend the study of inner-shell-vacancy production in ion-atom collisions to intermediate Z_1 and Z_2 values. The comparison between experiment and theory can be influenced by various factors, such as the distribution of charge and excitation states of projectiles moving in dense targets and multielectron effects in single collisions. Detailed molecular-orbital-model calculations may be too difficult to cope with this complexity. The statistical model gives a general framework for analysis and collation of such data for all shells and systems in a very general way. The scaling with atomic number of the coupling scheme in the MO model may overestimate the impact parameter at which P_K has a maximum in our Z_1, Z_2 domain. On the other hand, channels opened by the crossing of higher transient molecular orbitals, as subsummed by the statistical model, may have gained importance to such an extent that they, in fact, govern the vacancy-formation probabilities. As measurements are extended to larger Z_1 and Z_2, one may expect that the statistical model provides an increasingly effective basis for the prediction of inner-shell-vacancy production probabilities.

ACKNOWLEDGMENTS

This work was supported in part by the Division of Basic Energy Sciences, Department of Energy, under Contract No. EY-76-C-02-0016. Some of us (F.C.J., G.G., and T.H.K.) were Brookhaven National Laboratory Summer Visitors.

APPENDIX

We display the physical content of the statistical approach by treating inner-shell ionization as a random-walk process[22] of electron promotion between interacting level crossings of transient molecular orbitals. A comparison of the results of this simple approach with the results of the Mittleman and Wilets approach based on a diffusion equation show that essentially identical results are obtained. This demonstrates that the predictions of the statistical model do not depend

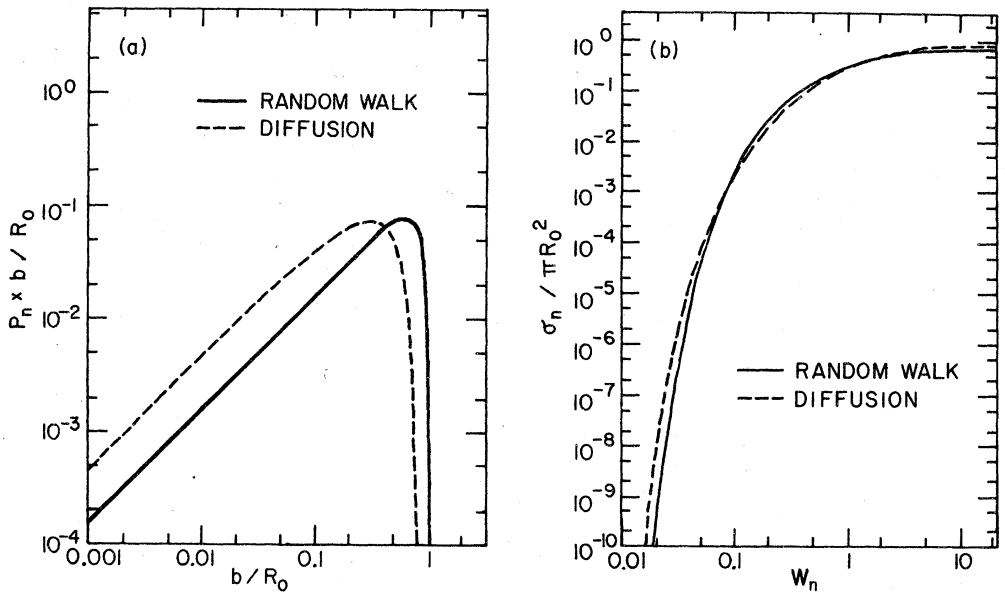

FIG. 7. Predictions of the statistical model in the random walk (——) and diffusion (---) approximation agree in essence. (a) Displays the product $P_n \times b/R_0$ of the probability for ionization of an inner-shell level n and the reduced impact parameter as a function of b/R_0. The solid curve is calculated from Eqs. (A3) and (A4) with $W_n = 1$, Eq. (A5), and the dashed curve from Eqs. (1) and (2) with $w_n = \frac{1}{3} W_n$. (b) Displays the reduced inner-shell vacancy-production cross section $\sigma_n/\pi R_0^2$ for a level n as a function of W_n. The solid curve is calculated from Eq. (A8), and the dashed curve from Eq. (4) with $w_n = \frac{1}{3} W_n$. By Eq. (A5), the abscissa values are equal to the reduced projectile velocities v/v_n for $2R_0 v_n/\overline{D}_n = 1$.

sensitively on the spacing of the transient molecular levels, nor on the detailed boundary conditions of the diffusion equation.

The probability dP_n that an electron starting from an energy level E_n at $t = 0$ will reach the threshold to unoccupied states $E_{\rm thr}$ during the time between t and $t + dt$ is given by

$$dP_n = \frac{\epsilon_n}{2t(\pi\delta t)^{1/2}} \exp\left(-\frac{\epsilon_n^2}{4\delta t}\right) dt, \tag{A1}$$

where $\epsilon_n = E_{\rm thr} - E_n$ and the electron-promotion parameter δ is related as $\delta = \frac{1}{2}\gamma\epsilon^2$, to γ, the mean number of level crossings per unit time between levels of average spacing ϵ. For $n = 1, 2$ we write also ϵ_K, ϵ_L, etc. Following Wilets,[20] one may set $\delta = C\dot{R}^2$, where $\dot{R}$ is the radial velocity during collision. The parameter C is treated as a constant when the internuclear distance R is less than an effective interaction range R_0 over which the atomic electron clouds interact strongly; and when $R > R_0$, $C \simeq 0$. We defer an extension of the treatment of excitations through rotational level coupling or "Coriolis mixing" via dependences of δ on the time-dependent angular velocity of the internuclear radius vector.

Without loss in generality, we can simplify matters by replacing the promotion parameter $\delta(t)$ by its value $\overline{\delta}(v, R_0)$ averaged over the collision time $t_{\rm col}$ and assume a straight projectile path with impact parameter b and constant velocity v. Integration of Eq. (1) over the collision time $t_{\rm col}$ given by

$$t_{\rm col} = (2R_0/v)(1 - x^2)^{1/2}\theta(1 - x) \tag{A2}$$

with $x \equiv b/R_0$ and

$$\theta(y) = (\tfrac{1}{2})(1 + y/|y|)$$

yields, in terms of the error function complement erfc, the ionization probability

$$P_n = \mathrm{erfc}(1/S_n^{1/2}), \tag{A3}$$

where

$$S_n = \frac{2R_0 v}{\overline{D}_n}\left(1 - \frac{b^2}{R_0^2}\right)^{1/2} \cdot \theta\left(1 - \frac{b^2}{R_0^2}\right) \equiv W_n(1 - x^2)^{1/2}\theta(1 - x^2), \tag{A4}$$

with the abbreviation

$$W_n = (2R_0 v_n/\overline{D}_n)(v/v_n), \tag{A5}$$

in terms of the orbital velocity v_n, and

$$\overline{D}_n = \epsilon_n^2 v^2/4\overline{\delta}. \tag{A6}$$

Since the mean promotion parameter in energy space, $\overline{\delta}$, is proportional to v^2, $\overline{D}_n$ is taken to be a constant and, because of its dimensions (L^2T^{-1}), is referred to as diffusion constant.

The total cross section becomes

$$\sigma_n = 2\pi R_0^2 \int_0^1 x\,dx P_n(x)$$

$$= 2\pi R_0^2 \int_1^\infty \frac{dy}{y^3} \operatorname{erfc}\left(\frac{y^{1/3}}{W_n^{1/2}}\right). \quad \text{(A7)}$$

We integrate and obtain to leading terms (with error <10%),

$$\sigma_n \simeq \pi R_0^2 \frac{2E_3(1/W_n)}{1+(\pi/W_n)^{1/2}}, \quad \text{(A8)}$$

where

$$E_3(x) = \int_1^\infty e^{-xt} t^{-3}\,dt .$$

Figure 7(a) is a comparison of Eq. (A3) with Eq. (1) and Fig. 7(b) is a comparison of Eq. (A8) with Eq. (4). The two approaches lead to essentially the same-impact-parameter and velocity dependencies. The coefficients $\bar{D}_n$ and D_n in the two approximations differ merely by a model-dependent numerical factor of the order of 1.

---

*Permanent address: Department of Physics, New York University, New York, N. Y. 10003.

[1]F. C. Jundt, H. Kubo, and K. H. Purser, in *Proceedings of the International Conference on Inner Shell Ionization Phenomena and Future Applications*, edited by R. W. Fink, S. T. Manson, J. M. Palms, and P. V. Rao (U.S. ERDA, Oak Ridge, Tenn., 1973), p. 1450; H. Kubo, F. C. Jundt, and K. H. Purser, Phys. Rev. Lett. 31, 674 (1973); H. Kubo, Ph.D. thesis (University of Rochester) (unpublished).

[2]W. E. Meyerhof, R. Anholt, T. K. Saylor, S. M. Lazarus, and A. Little, Phys. Rev. A 14, 1653 (1976); W. E. Meyerhof, R. Anholt, and T. K. Saylor, *ibid.* 16, 169 (1977); R. Anholt and W. E. Meyerhof, *ibid.* 16, 190 (1977).

[3]K. W. Jones, F. C. Jundt, G. Guillaume, and P. Fintz, in *Proceedings of the Tenth International Conference on the Physics of Electron and Atomic Collisions*, edited by M. Barat and J. Reinhardt (Commisariat à l'Energie Atomique, France, 1977), p. 528; K. W. Jones, F. C. Jundt, G. Guillaume, P. Fintz, and B. M. Johnson (unpublished).

[4]H. O. Lutz, in *Proceedings of the Second International Conference on Inner-Shell Ionization Phenomena*, edited by W. Melhorn and R. Brenn (University of Freiburg, Germany, 1976), p. 104.

[5]K. W. Jones, H. W. Kraner, and W. Brandt, Phys. Lett. 57A, 33 (1976).

[6]W. Brandt, and K. W. Jones, Phys. Lett. 57A, 35 (1976), and references cited therein.

[7]B. M. Johnson, K. W. Jones, and D. J. Pisano, Phys. Lett. 59A, 21 (1976); B. M. Johnson, K. W. Jones, W. Brandt, F. C. Jundt, G. Guillaume, and T. H. Kruse, in Ref. 3, p. 326.

[8]C. L. Cocke, R. R. Randall, S. L. Varghese, and B. Curnutte, Phys. Rev. A 14, 2026 (1976).

[9]J. M. Hansteen, *Advances in Atomic and Molecular Physics*, edited by D. R. Bates and B. Bederson, (Academic, New York, 1975), Vol. II, p. 299.

[10]W. Brandt and R. Laubert, Phys. Rev. Lett. 24, 1037 (1970).

[11]U. Fano and W. Lichten, Phys. Rev. Lett. 14, 627 (1965).

[12]M. Barat and W. Lichten, Phys. Rev. A 6, 211 (1972).

[13]J. S. Briggs, and J. H. Macek, J. Phys. B 5, 579 (1972); 6, 982 (1973).

[14]K. Taulbjerg, J. S. Briggs, and J. Vaaben, J. Phys. B 9, 1351 (1976).

[15]M. H. Mittleman and L. Wilets, Phys. Rev. 154, 12 (1967).

[16]R. Schuch, J. Volpp, I. Tserruya, K. E. Stiebing, R. Schule, H. Schmidt-Böcking, and G. Gaukler, in Ref. 3, p. 330; I. Tserruya, H. Schmidt-Böcking, and R. Schuch, Phys. Rev. A 18, (1978).

[17]W. Bambynek, B. Crasemann, R. W. Fink, H. U. Freund, H. Mark, C. D. Swift, R. E. Price, and V. P. Rao, Rev. Mod. Phys. 44, 716 (1972).

[18]L. Meyer, Phys. Status Solidi B 44, 253 (1971).

[19]N. Stolterfoht, D. Schneider, R. Mann, and F. Folkmann, J. Phys. B 10, L281 (1977), and references cited.

[20]L. Wilets, in *Proceedings of the Second International Conference on The Physics of Electronic and Atomic Collisions* (Benjamin, New York, 1961), p. 47; Phys. Rev. 116, 372 (1959).

[21]W. E. Meyerhof, Phys. Rev. Lett. 31, 1341 (1973).

[22]S. Chandrasekhar, Rev. Mod. Phys. 15, 1 (1943).